

# Ferromagnetic insulating phase in $\text{Pr}_{1-x}\text{Ca}_x\text{MnO}_3$

R. Kajimoto\*

*Department of Physics, Ochanomizu University, Bunkyo-ku, Tokyo 112-8610, Japan*

H. Mochizuki and H. Yoshizawa

*Neutron Science Laboratory, Institute for Solid State Physics,  
University of Tokyo, Tokai, Ibaraki 319-1106, Japan*

S. Okamoto†

*Institute of Physical and Chemical Research (RIKEN), Saitama 351-0198, Japan*

S. Ishihara

*Department of Physics, Tohoku University, Sendai 980-8578, Japan*

(Dated: May 6, 2018)

A ferromagnetic insulating (FM-I) state in  $\text{Pr}_{0.75}\text{Ca}_{0.25}\text{MnO}_3$  has been studied by neutron scattering experiment and theoretical calculation. The insulating behavior is robust against an external magnetic field, and is ascribed to neither the phase separation between a ferromagnetic metallic (FM-M) phase and a non-ferromagnetic insulating one, nor the charge ordering. We found that the Jahn-Teller type lattice distortion is much weaker than  $\text{PrMnO}_3$  and the magnetic interaction is almost isotropic. These features resembles the ferromagnetic metallic state of manganites, but the spin exchange interaction  $J$  is much reduced compared to the FM-M state. The theoretical calculation based on the staggered type orbital order well reproduces several features of the spin and orbital state in the FM-I phase.

PACS numbers: 75.47.Lx, 75.47.Gk, 75.25.+z, 75.30.Ds

## I. INTRODUCTION

Since the discovery of the high- $T_c$  superconductivity in layered cuprates, doped Mott insulators with perovskite structures become one of the major targets in recent studies of condensed matter physics. Hole doped perovskite manganites,  $R_{1-x}A_x\text{MnO}_3$  ( $R$  is a trivalent rare-earth ion and  $A$  is a divalent alkaline-earth ion), have been extensively studied since the discovery of the colossal magnetoresistance (CMR) effect. Recent studies devoted to clarify an origin of the CMR effect have revealed that the physics of manganites is controlled by an interplay between spin, charge and orbital degrees of freedom.

At  $x = 0$  in  $R_{1-x}A_x\text{MnO}_3$ , a Mn ion shows an electron configuration of  $t_{2g}^3e_g^1$  where the  $e_g$  orbital degree of freedom is active. Actually, the mother compound  $\text{RMnO}_3$  shows an alternate ordering of the  $d_{3x^2-r^2}$  and  $d_{3y^2-r^2}$  orbitals associated with the cooperative Jahn-Teller distortion in the  $ab$  plane of the orthorhombic  $Pbnm$  lattice. The layer-type ( $A$ -type) antiferromagnetic (AF) spin ordering is realized at low temperature by the anisotropic superexchange interaction under the orbital ordering (OO).<sup>1,2,3</sup> This anisotropy was experimentally confirmed in  $\text{LaMnO}_3$  by neutron scattering studies.<sup>4,5</sup> By substituting  $R$  by  $A$  in  $\text{RMnO}_3$ , holes are introduced in the system. In the simple double exchange scenario, a kinetic energy gain of the doped holes brings about the ferromagnetic metallic (FM-M) ground state.<sup>3,6</sup> It is also supposed that the OO is destroyed and the orbital liquid/disordered states are realized in the FM-M phase.<sup>7</sup> The isotropic characters in the crystal lattice<sup>8</sup> and the

spin exchange interactions<sup>9,10</sup> realized in this phase may be attributed to this orbital state.

However, in the actual compounds, the doping dependence of the electronic ground state is not so naive. Between the  $A$ -type AF phase and the FM-M phase, the ground state is ferromagnetic but insulating.<sup>3</sup> The ferromagnetic insulating (FM-I) state can not be explained by the simple double exchange picture. Although such a contradiction remains to be solved, the FM-I phase has not been much studied so far. This paper provides a detailed information about the character of the FM-I phase by a neutron scattering study and a theoretical calculation on  $\text{Pr}_{1-x}\text{Ca}_x\text{MnO}_3$ , which is a typical example for a FM-I phase with a relatively wide hole concentration region  $0.15 < x < 0.3$ .<sup>11</sup>

One of the interpretations of the FM-I phase is based on a phase separation between the FM-M phase and a non-FM insulating phase. In a recent trend of the research of CMR manganites, the phase separation phenomenon is regarded as an important factor for the large resistivity change accompanied by the insulator-metal (I-M) transition. A plausible origin of the non-FM insulating phase is the  $CE$ -type charge ordering (CO). This is a checkerboard-type CO of  $\text{Mn}^{3+}$  and  $\text{Mn}^{4+}$  accompanied by a zig-zag ordering of  $d_{3x^2-r^2}$  and  $d_{3y^2-r^2}$  orbitals on  $\text{Mn}^{3+}$  sites and the  $CE$ -type AF spin ordering. The  $CE$ -type CO is most stabilized at  $x = 1/2$ , but it is exceedingly robust against hole doping. Actually, in  $\text{Pr}_{1-x}\text{Ca}_x\text{MnO}_3$ , the  $CE$ -type CO is well developed for  $x \geq 0.3$  adjacent to the FM-I phase, and coexists with the FM component.<sup>11,12,13</sup> Recently, Dai *et al.* showed

by neutron scattering measurement that the short-range order of the  $CE$ -type CO exists in the FM-I phase of  $\text{La}_{1-x}\text{Ca}_x\text{MnO}_3$ ,<sup>14</sup> though the detail relation between these charge correlations and the transport is not obvious.

The phase separation picture requires substantial volume fraction of non-FM insulating phase to make the compound an insulator overcoming the metallic conduction in the FM phase. Uehara *et al.* studied the phase separation between the FM-M phase and the charge-ordered insulating (CO-I) phase in  $\text{La}_{5/8-y}\text{Pr}_y\text{Ca}_{3/8}\text{MnO}_3$ . They showed that the concentration of the FM-M phase at the I-M transition, which was evaluated from the ratio of the saturation magnetic moment to the full moment of a Mn ion, agrees with the three-dimensional (3D) percolation threshold 10–25%.<sup>15</sup> However, the FM moment of  $\sim 2 \mu_B$  in  $\text{Pr}_{0.7}\text{Ca}_{0.3}\text{MnO}_3$ <sup>12,13,16</sup> is too large to account for its insulating character. On the other hand, there is another possibility that the insulating nature does not arise from the non-FM phase but it is intrinsic to the FM phase. Recently several kinds of COs related to the hole concentration of  $x = 1/4$  were theoretically proposed. Hotta *et al.* claimed that  $\text{Pr}_{3/4}\text{Ca}_{1/4}\text{MnO}_3$  becomes a FM-I state by a CO consisting of a checkerboard charge ordered plane and a purely  $\text{Mn}^{3+}$  plane stacking alternately along the  $z$  axis.<sup>17</sup> As a result, the unit cell of the CO becomes  $\sqrt{2} \times \sqrt{2} \times 4$  in terms of the cubic perovskite unit (We will refer this type of CO as  $(\pi, \pi, \pi/2)$ -type CO.). Mizokawa *et al.* proposed that in the lightly doped manganites there exist “orbital polarons.” Here  $\text{Mn}^{4+}$  ions are surrounded by ferromagnetically coupled nearest neighbor  $\text{Mn}^{3+}$  ions where the  $e_g$  orbitals are pointed to the central  $\text{Mn}^{4+}$  site.<sup>18</sup> They claimed that in  $\text{Pr}_{3/4}\text{Ca}_{1/4}\text{MnO}_3$ , the orbital polarons form a body-centered cubic lattice whose unit cell has a size of  $2 \times 2 \times 2$  in unit of the cubic perovskite lattice, and a FM insulator is realized.<sup>19</sup> Neither kind of CO, however, has not been detected experimentally so far. Instead, Endoh *et al.* claimed by resonant x-ray scattering (RXS) and neutron scattering studies that the FM-I phase of  $\text{La}_{0.88}\text{Sr}_{0.12}\text{MnO}_3$  shows an OO of a mixture of  $d_{3z^2-r^2}$  and  $d_{x^2-y^2}$  orbitals. They also proposed that this OO is an origin of the FM-I state.<sup>20,21</sup> As for the orbital state of the FM-I phase in  $\text{Pr}_{1-x}\text{Ca}_x\text{MnO}_3$ , Zimmermann *et al.* advocated by a RXS study that the same OO as that in  $\text{LaMnO}_3$  ( $\text{LaMnO}_3$ -type OO) develops below about 500 K in  $\text{Pr}_{0.75}\text{Ca}_{0.25}\text{MnO}_3$ .<sup>22</sup> In contrast to the FM spin ordering in  $\text{Pr}_{0.75}\text{Ca}_{0.25}\text{MnO}_3$ , however,  $\text{LaMnO}_3$ -type OO is generally accompanied with the  $A$ -type AF spin ordering.

The complicated status of the current research on the FM-I state of manganites reminds us the necessity of a comprehensive study on spin, charge, and orbital states of the FM-I phase of manganites. For this purpose, neutron scattering is a useful tool to study CO and OO because of its sensitivity to the lattice distortions induced by CO and OO. In the present study, we performed elas-

tic neutron scattering measurements on a single crystal of  $\text{Pr}_{0.75}\text{Ca}_{0.25}\text{MnO}_3$  to elucidate the superlattice peaks and the lattice distortions due to CO and OO. The OO affects the exchange interactions between spins due to the anisotropic character of the  $e_g$  orbitals. Therefore, through the estimation of the exchange interactions by measuring the magnon dispersion relation, we can characterize the orbital state. So, we also performed inelastic neutron scattering measurements to determine the spin exchange through the measurements of the spin wave excitations. The theoretical analyses provide a unified picture for the spin and orbital states in the AF, FM-I and FM-M phases.

The rest of this paper is organized as follows. In the next section the experimental procedure is described. The results and discussions are described in Sec. III, where the property of the magnetic and crystal structures in  $\text{Pr}_{0.75}\text{Ca}_{0.25}\text{MnO}_3$  are discussed. In Sec. III-A, we will argue the possibility of the phase separation, and in Sec. III-B we will characterize the FM-I state by measurements of the structural properties and spin fluctuations. Section III-C is devoted to the theoretical investigation for the magnetic interaction and the orbital state in moderately doped manganites. A summary of the work is given in Sec. V.

## II. EXPERIMENTAL PROCEDURES

Single crystals of  $\text{Pr}_{0.75}\text{Ca}_{0.25}\text{MnO}_3$  and  $\text{PrMnO}_3$  were grown by the floating zone method. A stoichiometric mixture of  $\text{Pr}_6\text{O}_{11}$ ,  $\text{CaCO}_3$ , and  $\text{Mn}_3\text{O}_4$  was ground and calcined at 1300 °C in air for 12 h. Then the resulting powder was pressed into rods and fired again at 1300 °C in air for 12 h. The crystal growth was performed in a floating-zone furnace in a flow of oxygen gas. We precharacterized the samples by a powder x-ray diffraction measurement and confirmed that the samples are single phase. Then the samples were cut into the size of  $6 \text{ mm}\phi \times 30 \text{ mm}$  for the present neutron scattering study. The transport data were taken using Quantum Design PPMS on a sample cut from the same batch as used in the neutron study.

The neutron scattering experiments were performed using triple axis spectrometers GPTAS and HQR of Institute for Solid State Physics, University of Tokyo, installed at the JRR-3M research reactor in JAERI, Tokai, Japan. The most of the measurements were done at GPTAS, while HQR was utilized when a high  $Q$  resolution was required. At both spectrometers, the 002 reflection of pyrolytic graphite (PG) was used for the monochromator and analyzer. At GPTAS, we selected a neutron wave length of  $k_f = 3.81 \text{ \AA}^{-1}$ . For elastic scattering measurements, a combination of horizontal collimators of 20'-40'-40'-80' (from reactor to detector) was adopted and two PG filters were placed before the monochromator and after the sample to suppress contaminations of higher-order harmonics. For inelastic scattering measurements,

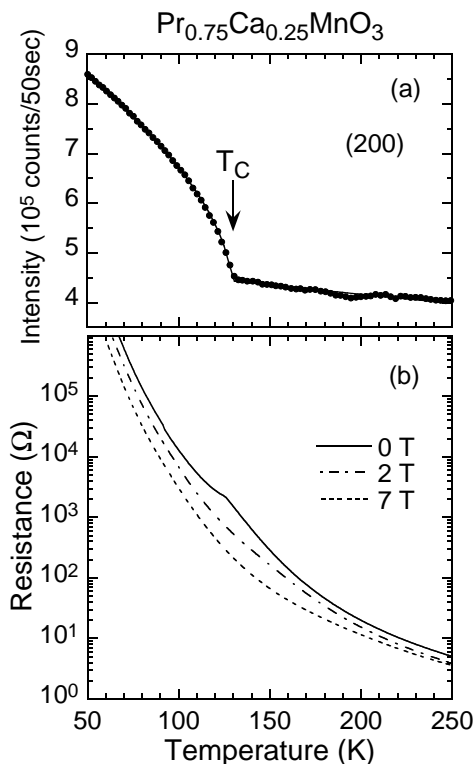


FIG. 1: (a) Temperature dependence of the scattering intensity of the 200 peak. (b) Temperature dependence of the resistance under the magnetic field of  $H = 0$  T, 2 T, and 7 T.

we chose 40'-40'-40'-40' combination of collimators and set a PG filter after the sample. At HQR, which is on the thermal guide tube, neutrons of wave length  $k_i = 2.56 \text{ \AA}^{-1}$  and horizontal collimation of blank-40'-80' (from monochromator to sample) were used together with a PG filter before the sample. The crystals were mounted in aluminum cans filled with helium gas. The temperature of the samples were controlled by conventional and high-temperature-type closed cycle He-gas refrigerators. The measurements were performed in the  $(h, 0, l)$  and  $(h, h, l)$  zones of reciprocal space of the  $Pbnm$  lattice.

### III. RESULTS AND DISCUSSIONS

#### A. Possibility of the phase separation

First, let us characterize the sample by showing the results of the temperature ( $T$ ) dependences of the order parameter of the magnetic order and the resistance. Figure 1(a) is the  $T$  dependence of the scattering intensity of the fundamental 200 peak. The intensity starts to increase below the Curie temperature  $T_C \sim 130$  K due to the FM spin ordering, consistent with a previous study.<sup>11</sup> To determine the critical exponent, we fit the data to a power law,  $(1 - T/T_C)^{2\beta}$ , varying the lower limit of the temperature range of the fitting,  $T_{\text{lim}}$ .  $\beta$  was

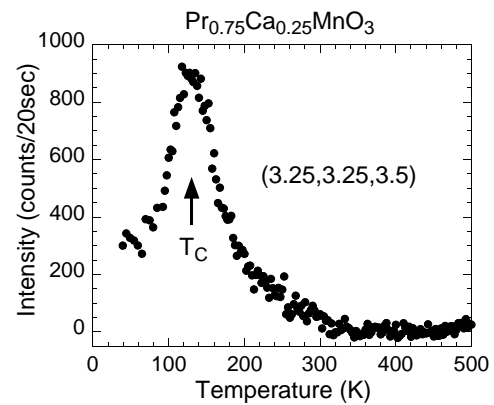


FIG. 2: Temperature dependence of the intensity of the CE-type charge/orbital order peak at  $Q = (3.275, 3.275, 3.55)$ . The intensity due to the Huang scattering measured at  $Q = (3.33, 3.33, 3.66)$  is subtracted.

determined to be  $0.36(1)$  as  $T_{\text{lim}} \rightarrow T_C = 129.5(5)$  K. This value of the critical exponent is very close to that for the 3D FM Heisenberg model,  $0.367$ , and similar to that for the FM-M manganites such as  $\text{La}_{0.7}\text{Sr}_{0.2}\text{MnO}_3$ <sup>23</sup> and  $\text{La}_{0.7}\text{Sr}_{0.3}\text{MnO}_3$ .<sup>9,23</sup> The magnetic moment was determined from a powder sample which was prepared by crushing a melt-grown crystal. The FM moment is  $3.32(3) \mu_B$  per Mn site at 15 K, oriented parallel to the  $b$  axis. This value of the FM moment is nearly equal to the formula value of  $3.75 \mu_B$ . This means that even if a non-FM region existed in the sample, its volume would be extremely small.

Figure 1(b) shows the  $T$  dependence of the resistance at several magnetic fields. For  $H = 0$  T, the sample is insulating for all temperature range measured, and a small cusp is observed at  $T_C$ . By applying the magnetic field, this cusp vanishes, and the resistance is reduced from that at  $H = 0$  T. However the insulating behavior still persists under the magnetic field up to  $H = 7$  T. The robustness of the insulating state contrasts markedly with the CE-type charge ordered phase for  $x > 0.3$ , where the CO melts by a magnetic field of a few teslas.<sup>11</sup> In the present case, because the spins are already fully aligned ferromagnetically at  $H = 0$  T, an external field cannot make a significant change of the transports.

As mentioned above, the magnetic and transport properties suggest that the insulating behavior of  $\text{Pr}_{0.75}\text{Ca}_{0.25}\text{MnO}_3$  does not originate from the non-FM region, but it is rather intrinsic to the FM state. To confirm this point, we performed the neutron diffraction measurements and surveyed reciprocal points to detect signals due to the CE-type CO, and found the lattice superlattice peaks due to the CE-type CO. Figure 2 shows a  $T$  dependence of the scattering intensity at  $Q = (3.25, 3.25, 3.5)$ , which corresponds to a CE-type CO peak  $(5, 1.5, 0)$ <sup>24</sup> of a different domain of the sample. Because diffuse scattering due to single polarons (Huang scattering) overlaps at this position,<sup>26</sup> the intensity of the diffuse scattering estimated at  $Q = (3.33, 3.33, 3.66)$

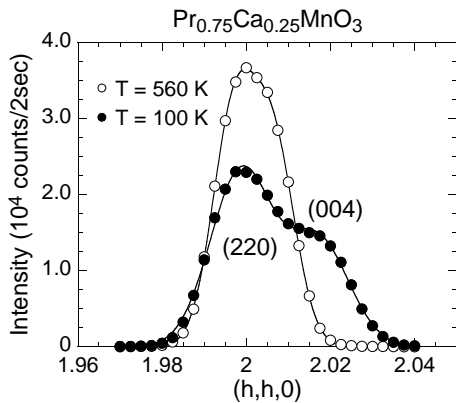


FIG. 3: Profiles of the 220/004 doublet along the [110] direction at 100 K and 560 K. The data are collected at the HQR spectrometer. Solid lines are fits to two Gaussians.

is subtracted from the data, and intensity of 100 counts is added to compensate the difference in background intensity at the two positions. The *CE*-type CO develops below  $T \sim 320$  K. It is drastically suppressed below  $T_C$ , although the sample remains insulating [Fig. 1(b)]. The small cusp of the resistance at  $T_C$  may be related to the melting of the *CE*-type CO, but the overall insulating feature of the resistance, however, cannot be explained by the *CE*-type CO. This is in contrast to the FM-M region of manganites, where the disappearance of the short-range *CE*-type CO accompanies the transition to the FM-M state.<sup>14,26,27</sup> We think that the existence of the *CE*-type CO is due to a small mixture of a higher Ca concentration phase. We also found the pseudo *CE*-type AF peaks concomitant with the *CE*-type CO in the region of  $x < 1/2$ .<sup>12,13,16,28</sup> Their intensity is of the order of  $10^{-3}$  in comparison with that of the FM peak, indicating that the volume of the *CE*-type CO phase is negligible.

### B. Character of the homogeneous FM-I state

The results described in the previous section indicates the phase separation between the FM-M phase and the non-FM insulating phase is not important for the FM-I phase of  $\text{Pr}_{1-x}\text{Ca}_x\text{MnO}_3$ . The FM-I state is an intrinsic state of the low doped region of manganites. Consequently, to understand the *homogeneous* FM-I phase, we will characterize the charge and orbital states in this phase.

First, we tried to clarify whether the FM-I state is a FM charge ordered state as theoretically proposed. For the  $(\pi, \pi, \pi/2)$ -type CO proposed by Hotta *et al.*,<sup>17</sup> the superlattice peaks are expected at  $\mathbf{Q} = (h, k, l)$  with  $h + k = \text{odd}$  and  $l = \text{half integer}$ . To detect this type of CO, we surveyed  $(m, 0, 1/2)$  and  $(5, 0, n/2)$  positions where  $m$  and  $n$  are odd integer, but could not find any peaks. This result is negative for the existence of this type of charge order in  $\text{Pr}_{0.75}\text{Ca}_{0.25}\text{MnO}_3$ .

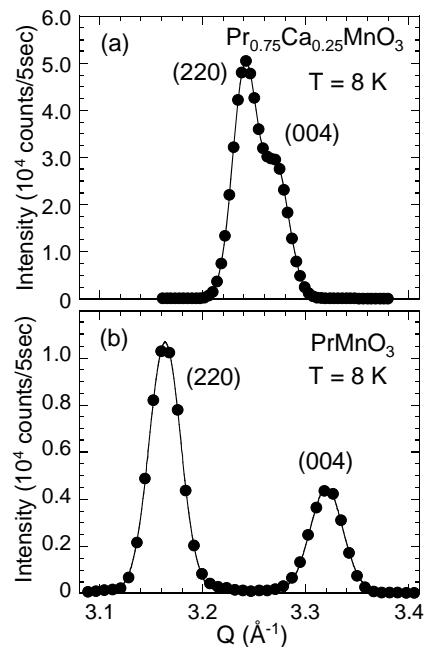


FIG. 4: Profiles of the 220/004 doublets along the [110] direction for (a)  $\text{Pr}_{0.75}\text{Ca}_{0.25}\text{MnO}_3$  and (b) for  $\text{PrMnO}_3$  at 8 K. The horizontal axes indicate the amplitudes of the scattering vector  $\mathbf{Q}$ . Solid lines are fits to two Gaussians.

The orbital polaron lattice proposed by Mizokawa *et al.*<sup>18,19</sup> will produce superlattice reflections at  $\mathbf{Q} = (h, k, l)$  with  $(h + k = \text{odd and } l = \text{even})$  or  $(h, k = \text{half integer and } l = \text{odd})$ . We found peaks at several positions satisfying these conditions and forbidden by the *Pbnm* symmetry. Unfortunately, however, these positions coincide with those with integer indices considering the twinning of the crystal. Because additional small tilts of  $\text{MnO}_6$  octahedra can produce Bragg peaks at such positions, we cannot determine whether the orbital polaron lattice exists or not from the present study, though no clear relation between the intensities of these peaks and the resistance was observed.

Next, we will investigate the orbital state of the FM-I state. According to the recent RXS study, resonant signals observed in  $\text{Pr}_{0.75}\text{Ca}_{0.25}\text{MnO}_3$  is consistent to the same OO as  $\text{LaMnO}_3$ , i.e. alternate ordering of  $d_{3x^2-r^2}$  and  $d_{3y^2-r^2}$  orbitals in the *ab* plane.<sup>22</sup>  $\text{LaMnO}_3$ -type OO is expected to produce significant anisotropies in crystal structure as well as spin exchange: The in-plane lattice constants  $a$  and  $b$  become longer than the out-of-plane lattice constant  $c$ , and the exchange interactions within the *ab* plane will be stronger than that along the  $c$  axis. Therefore, measuring these quantities should be useful for quantitative understanding of the orbital state.

Figure 3 shows neutron diffraction profiles around the fundamental (2,2,0) position along the [110] direction at 100 K and 560 K. Because of the twinning, the 004 peak is also observed at slightly higher  $Q$  than the 220 peak. At  $T = 560$  K, both peaks locate so close that the observed profile forms almost a single peak. On the other hand,

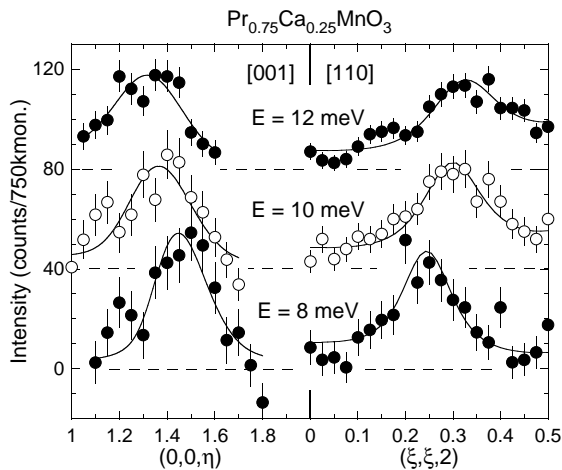


FIG. 5: Profiles of constant-energy scan of the magnon spectra along the [001] direction (left) and the [110] direction (right). The background is subtracted from each data. The vertical axes are shifted by 40 counts for each energy. Solid lines are fits to the Lorentzian spectral function convoluted with the instrumental resolution.

this peak splits into two peaks at  $T = 100$  K due to small increase of the  $a$  or  $b$  axis and large decrease of the  $c$  axis. This change of the lattice constants is consistent to the cooperative Jahn-Teller distortions accompanied by the LaMnO<sub>3</sub>-type OO. We measured  $T$  dependences of similar profiles and found that the structural change gradually develops below  $\sim 450$  K. This temperature coincides with the temperature where the orbital signals measured by the RXS study starts to increase,<sup>22</sup> and corresponds to the transition temperature from the  $O$  phase to the  $O'$  phase identified in Ref. 28. These results qualitatively suggest the developing of the LaMnO<sub>3</sub>-type OO below  $T \sim 450$  K. However, the amplitude of the lattice distortion is fairly small compared to the mother compound, PrMnO<sub>3</sub>, where a typical LaMnO<sub>3</sub>-type OO is expected. This can easily be assured by comparing the profile of the 220/004 reflections for both compounds. In Fig. 4, we depicted the profiles of the 220 and 004 reflections of Pr<sub>0.75</sub>Ca<sub>0.25</sub>MnO<sub>3</sub> [Fig. 4(a)] and PrMnO<sub>3</sub> [Fig. 4(b)] at  $T = 8$  K. We show the amplitude of the scattering vector  $Q$  as the horizontal axis for easier comparison of two data.

Figure 5 is typical profiles of constant-energy scans of spin wave excitations along the out-of-plane direction [001] (left panel) and the in-plane direction [110] (right panel) of Pr<sub>0.75</sub>Ca<sub>0.25</sub>MnO<sub>3</sub>. The data were collected near the FM Bragg point (0,0,2) at  $T = 8$  K. The magnetic origin of these excitations were confirmed by measuring their  $Q$  dependence. The peak positions get away from the zone center as the energy increases according to the dispersion relation of the spin wave. From these measurements, we obtained the dispersion relation of the spin wave along the two directions, which is shown in Fig. 6. Note that the momentum transfer  $\mathbf{q} = (0, 0, 2n)$  has almost the same magnitude as

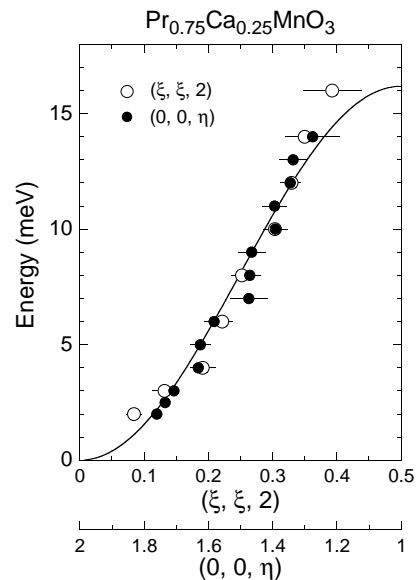


FIG. 6: Spin wave dispersion relations in Pr<sub>0.75</sub>Ca<sub>0.25</sub>MnO<sub>3</sub> along the [110] and [001] directions at 8 K. Solid line is a dispersion curve for the FM Heisenberg model with an isotropic nearest neighbor coupling.

$\mathbf{q} = (n, n, 0)$  in the  $Pbnm$  notation. In contrast to the LaMnO<sub>3</sub>,<sup>4,5</sup> two dispersion curves well coincide, indicating that the spin exchange is isotropic ( $J_{ab} \sim J_c$ ). This is consistent to the critical exponent  $\beta$  [Sec. III-A], which is almost the same as the value for a 3D system. The observed dispersion curves can be described by the conventional FM Heisenberg model:  $\mathcal{H} = -\sum_{ij} J_{ij} \mathbf{S}_i \cdot \mathbf{S}_j$ , where  $J_{ij}$  is the exchange integral between spins at site  $\mathbf{R}_i$  and  $\mathbf{R}_j$ . In the linear approximation, the dispersion relation is given by  $\hbar\omega(\mathbf{q}) = \Delta + 2S[J(\mathbf{0}) - J(\mathbf{q})]$ , where  $J(\mathbf{q}) = \sum_j J_{ij} \exp[i\mathbf{q} \cdot (\mathbf{R}_i - \mathbf{R}_j)]$  and  $\Delta$  accounts for small anisotropies. Taking only the isotropic nearest neighbor coupling  $J$  into account is sufficient to reproduce the observed data, and we get the solid line in Fig. 6 with  $2JS = 4.0(2)$  meV and  $\Delta = 0.0(3)$  meV.

The isotropic character of the spin system shows an interesting resemblance among the orbital-ordered FM-I phase and the orbital-disordered FM-M phase. However, one can distinguish them by the magnitude of the spin exchange. Clear enhancement of the spin stiffness  $D(T)$  on the transition from the FM-I phase to the FM-M phase has been observed in a hole concentration dependence of La<sub>1-x</sub>Sr<sub>x</sub>MnO<sub>3</sub><sup>29</sup> and La<sub>1-x</sub>Ca<sub>x</sub>MnO<sub>3</sub><sup>30</sup> by neutron scattering studies. The same phenomenon on the field-induced I-M transition in Pr<sub>0.7</sub>Ca<sub>0.3</sub>MnO<sub>3</sub> has also been observed.<sup>31</sup> In these materials,  $D(0)$  in the insulating phase is  $\approx 50$  meV $\text{\AA}^2$  and that in the metallic phase is  $\approx 150$  meV $\text{\AA}^2$ . If we estimate  $D(0)$  of the present Pr<sub>0.75</sub>Ca<sub>0.25</sub>MnO<sub>3</sub> compound from  $J$  at 8 K by a relation  $D = 2JSa_c^2$  where  $a_c$  is the lattice constant of the cubic lattice,  $D(0)$  becomes  $\approx 60$  meV $\text{\AA}^2$ . This value is almost same as that of the insulating La<sub>1-x</sub>Sr<sub>x</sub>MnO<sub>3</sub>, La<sub>1-x</sub>Ca<sub>x</sub>MnO<sub>3</sub>, and Pr<sub>0.7</sub>Ca<sub>0.3</sub>MnO<sub>3</sub>. This fact evi-

dences the common ground of the FM-I phase of the manganites.

The Jahn-Teller type lattice distortion means that there may exist a LaMnO<sub>3</sub>-like OO as reported by the RXS study. Its smallness and the isotropy in  $J$ , however, suggest that the electron distribution is more isotropic than that in the LaMnO<sub>3</sub>-type OO. Similar situation is realized in the FM-I phase of La<sub>0.88</sub>Sr<sub>0.12</sub>MnO<sub>3</sub>,<sup>20,32</sup> where the staggered orbital ordering of  $(|d_{3z^2-r^2}\rangle \pm |d_{x^2-y^2}\rangle)/\sqrt{2}$  is proposed.<sup>20,21</sup> In the next section, we will theoretically investigate the orbital state Pr<sub>1-x</sub>Ca<sub>x</sub>MnO<sub>3</sub> and construct the spin and orbital phase diagram.

### C. Theory

Spin and orbital states in manganites with moderate hole doping are examined theoretically from the view point of strong electron correlation. We adopt the  $t$ - $J$  type Hamiltonian where the double degeneracy of the  $e_g$  orbitals is taken into account. The model Hamiltonian consists of the following four terms:<sup>33</sup>

$$\mathcal{H} = \mathcal{H}_t + \mathcal{H}_J + \mathcal{H}_H + \mathcal{H}_{AF}. \quad (1)$$

The first and second terms are the main terms corresponding to the  $t$  and  $J$  terms in the  $t$ - $J$  model, respectively, given by

$$\mathcal{H}_t = \sum_{\langle ij \rangle \gamma \gamma' \sigma} t_{ij}^{\gamma \gamma'} \tilde{d}_{i\gamma\sigma}^\dagger \tilde{d}_{j\gamma'\sigma} + H.c., \quad (2)$$

and

$$\begin{aligned} \mathcal{H}_J = & -2J_1 \sum_{\langle ij \rangle} \left( \frac{3}{4} n_i n_j + \vec{S}_i \cdot \vec{S}_j \right) \left( \frac{1}{4} - \tau_i^l \tau_j^l \right) \\ & - 2J_2 \sum_{\langle ij \rangle} \left( \frac{1}{4} n_i n_j - \vec{S}_i \cdot \vec{S}_j \right) \left( \frac{3}{4} + \tau_i^l \tau_j^l + \tau_i^l + \tau_j^l \right) \end{aligned} \quad (3)$$

$\tilde{d}_{i\gamma\sigma}$  is the annihilation operator of the  $e_g$  electron at site  $i$  with orbital  $\gamma$  and spin  $\sigma$ . This operator is defined in the restricted Hilbert space where the  $e_g$  electron numbers at each Mn site are limited to be one or less. The prefactor  $t_{ij}^{\gamma \gamma'}$  is the transfer integral between orbital  $\gamma$  at site  $i$  and  $\gamma'$  at  $j$ .  $\mathcal{H}_J$  describes the superexchange interactions between the nearest neighboring Mn spins and orbitals. The spin and orbital degrees of freedom for the  $e_g$  electron are represented by the spin operator

$$\vec{S}_i = \frac{1}{2} \sum_{\gamma \sigma \sigma'} \tilde{d}_{i\gamma\sigma}^\dagger \vec{\sigma}_{\sigma \sigma'} \tilde{d}_{i\gamma\sigma'}, \quad (4)$$

and the pseudo-spin operator

$$\vec{T}_i = \frac{1}{2} \sum_{\gamma \gamma' \sigma} \tilde{d}_{i\gamma\sigma}^\dagger \vec{\sigma}_{\gamma \gamma'} \tilde{d}_{i\gamma'\sigma}, \quad (5)$$

respectively, with the Pauli matrices  $\vec{\sigma}$ .  $\tau_i^l$  in  $\mathcal{H}_J$  is defined by the pseudo-spin operator as

$$\tau_i^l = \cos\left(\frac{2m_l\pi}{3}\right) T_{iz} + \sin\left(\frac{2m_l\pi}{3}\right) T_{ix}, \quad (6)$$

with  $(m_x, m_y, m_z) = (1, 2, 3)$  where  $l (= x, y, z)$  indicates a direction of the bond connecting site  $i$  and site  $j$ . The magnitudes of the superexchange interactions  $J_1$  and  $J_2$  satisfy the condition  $J_1 > J_2 > 0$ . The third and fourth terms in the Hamiltonian Eq. (1) describe the Hund coupling  $J_H (> 0)$  between the  $e_g$  and  $t_{2g}$  spins

$$\mathcal{H}_H = -J_H \sum_i \vec{S}_i \cdot \vec{S}_{ti}, \quad (7)$$

and the AF superexchange interaction  $J_{AF} (> 0)$  between the nearest neighboring  $t_{2g}$  spins

$$\mathcal{H}_{AF} = J_{AF} \sum_{\langle ij \rangle} \vec{S}_{ti} \cdot \vec{S}_{tj}, \quad (8)$$

respectively.  $\vec{S}_{ti}$  is the spin operator for the  $t_{2g}$  electrons with  $S = 3/2$ . It was confirmed that this model is successful in description the spin and orbital ordered state in hole doped and undoped manganites.<sup>21,33</sup>

Here, we examine the orbital ordered and disordered states in the unified fashion by applying the generalized slave boson method. The electron annihilation operator  $\tilde{d}_{i\gamma\sigma}$  is decomposed into the holon  $h_i$ , spinon  $s_{i\sigma}$  and pseudo-spinon  $t_{i\gamma}$  operators as

$$\tilde{d}_{i\gamma\sigma} = h_i^\dagger s_{i\sigma} t_{i\gamma}, \quad (9)$$

with the local constraints of

$$h_i^\dagger h_i + \sum_\gamma t_{i\gamma}^\dagger t_{i\gamma} = 1, \quad (10)$$

and

$$\sum_\sigma s_{i\sigma}^\dagger s_{i\sigma} = \sum_\gamma t_{i\gamma}^\dagger t_{i\gamma}, \quad (11)$$

at each Mn site. We choose that both the holon and spinon are bosons, and the pseudo-spinon is a fermion.<sup>35,36,37</sup> This is because 1) in the ferromagnetic metallic phase, the hole carrier is recognized to be a fermion with orbital degree of freedom which is treated by  $h_i^\dagger t_{i\gamma}$ , and 2) the fermionic operator for the orbital degree of freedom  $t_{i\gamma}$  is suitable for describing the orbital disordered state. We adopt the mean field approximation where we take the bond order parameters for orbital

$$\sum_{\gamma \gamma'} \langle t_{ii+l}^{\gamma \gamma'} t_{i+l\gamma'}^\dagger \rangle = t_0 \chi_t^l, \quad (12)$$

and those for spin

$$\sum_\sigma \langle s_{i\sigma}^\dagger s_{i+l\sigma} \rangle = \chi_s^l, \quad (13)$$

and the site diagonal order parameters for orbital

$$\sum_{\gamma\gamma'} \langle t_{i\gamma}^\dagger \sigma_{\gamma\gamma}^\mu t_{i\gamma} \rangle = m_t^\mu(i), \quad (14)$$

for  $\mu = x$  and  $z$ , and those for spin

$$\sum_{\sigma} \langle s_{i\sigma}^\dagger \sigma_{\sigma\sigma}^z s_{i\sigma} \rangle = m_s^z(i). \quad (15)$$

$t_0$  in Eq. (12) is the electron transfer intensity between the nearest neighboring  $d_{3z^2-r^2}$  orbitals along the  $z$  axis. We also introduce a mean field for the holon

$$\langle h_i^\dagger h_i \rangle = - \langle h_i^\dagger h_j \rangle = x, \quad (16)$$

with the hole concentration  $x$ . In this scheme, the local constraints are released into the global ones:

$$\sum_i \left( h_i^\dagger h_i + \sum_{\gamma} t_{i\gamma}^\dagger t_{i\gamma} \right) = 1, \quad (17)$$

and

$$\sum_{i\sigma} s_{i\sigma}^\dagger s_{i\sigma} = \sum_{i\gamma} t_{i\gamma}^\dagger t_{i\gamma}. \quad (18)$$

By considering the strong Hund coupling  $J_H$ , the directions of  $\vec{S}_i$  and  $\vec{S}_{ti}$  are assumed to be the same. The effects of the lattice distortion and its coupling to the  $e_g$  electrons are not considered explicitly in the present model. This is because, in the moderately hole doped region of our interest, the Jahn-Teller distortion is significantly reduced as shown in the previous section.

The phase diagram is obtained numerically by minimizing the free energy with respect to the order parameters [Fig. 7]. The parameter values are chosen to be  $J_2/J_1 = 0.25$ ,  $J_{AF}/J_1 = 0.014$ , and  $t_0/J_1 = 2$ . For the Fourier transform of the site diagonal order parameters  $m_t^\mu(\vec{k})$  and  $m_s^z(\vec{k})$ , we assume that  $m_t^x(\pi\pi 0)$ ,  $m_t^z(000)$ ,  $m_s^z(00\pi)$  and  $m_s^z(000)$  are finite in the ordered phases. Below the orbital ordering temperature  $T_{OO}$ , the site diagonal orbital order parameters  $m_t^\mu(\vec{k})$  appear.  $T_C$  and  $T_N$  are the Curie temperature and the Néel temperature for the  $A$ -type AF order, respectively, where  $m_s^z(000)$  and  $m_s^z(00\pi)$  appear, respectively. At  $x = 0$ , the staggered type orbital order  $m_t^x(\pi\pi 0)$  occurs far above  $T_N$  as observed in  $\text{LaMnO}_3$  and  $\text{PrMnO}_3$ . By taking into account the cooperative Jahn-Teller effects which is not included in the present calculation,  $T_{OO}$  may increase from the calculated value. With doping of holes,  $T_{OO}$  rapidly decreases and disappears around  $x = 0.15$  ( $\equiv x_c$ ). Above  $x_c$ ,  $m_t^\mu(\vec{k})$  becomes zero, but the bond order parameters  $\chi_t^\mu(\vec{k})$  still remain finite. That is, the orbital liquid state is realized above the critical point  $x_c$ . As for the magnetic ordering, the  $A$ -type AF phase is changed into the FM phase through the canted AF one. The  $x$  dependence of  $T_C/T_N$  is almost flat below  $x = 0.1$  and

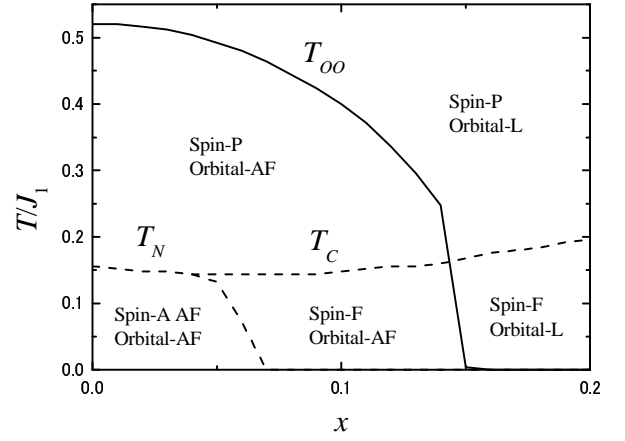


FIG. 7: The spin and orbital phase diagram in the hole concentration  $x$  and temperature  $T$  plane. The parameter values are chosen to be  $J_2/J_1 = 0.25$ ,  $J_{AF}/J_1 = 0.014$ , and  $t_0/J_1 = 2$ .  $F$ ,  $AF$ ,  $P$  and  $L$  indicate the ferromagnetic phase, the antiferromagnetic phase, the paramagnetic phase, and the orbital liquid phase, respectively.

slightly increases with increasing  $x$ . The ground state electronic phase are classified into (I) the (canted)  $A$ -type AF phase with the staggered OO corresponding to  $\text{LaMnO}_3$  and  $\text{PrMnO}_3$ , (II) the FM phase with the staggered OO which is discussed later in more detail, and (III) the FM phase with the orbital liquid state corresponding to the FM-M state in heavily hole doped manganites, such as  $\text{La}_{1-x}\text{Sr}_x\text{MnO}_3$  with  $x \sim 0.3$ . In a series of  $\text{Pr}_{1-x}\text{Ca}_x\text{MnO}_3$ , it is interpreted that this phase does not appear because the charge ordered AF insulating phase is stable down to the region of  $x \sim 0.3$  instead of this FM-M phase.

Now we focus on the FM phase with the staggered OO. We interpret that this corresponds to the FM phase in  $\text{Pr}_{1-x}\text{Ca}_x\text{MnO}_3$  with  $0.15 < x < 0.3$  of our present interest. The OO in this FM phase is of the staggered type where the two kinds of orbital are characterized by the orbital mixing angles  $(\theta/ -\theta)$ , as well as the OO in the  $A$ -type AF phase. This angle is defined as  $|\theta\rangle = \cos\frac{\theta}{2}|d_{3z^2-r^2}\rangle + \sin\frac{\theta}{2}|d_{x^2-y^2}\rangle$ . This is consistent with the azimuthal angle scan of the RXS experiments in  $\text{Pr}_{0.75}\text{Ca}_{0.25}\text{MnO}_3$ ; the azimuthal angle  $\varphi$  is the rotation angle of the sample around the x-ray scattering vector  $\vec{k}_i - \vec{k}_f$  in the RXS experiments. By measuring the  $\varphi$  dependence of the RXS intensity  $I(\varphi)$ , the information for the symmetry of the orbital ordered states is deduced.<sup>34</sup> The experimentally observed  $I(\varphi)$  in  $\text{Pr}_{0.75}\text{Ca}_{0.25}\text{MnO}_3$  is proportional to a function  $\sin^2\varphi$  which is consistent with the theoretical prediction for  $I(\varphi)$  in the OO state of the  $(\theta/ -\theta)$  type.<sup>22,34</sup> The value of  $\theta$  in the present calculation is about  $\pi$ . That is, the orbital wave functions are given by  $(|d_{3z^2-r^2}\rangle \pm |d_{x^2-y^2}\rangle)/\sqrt{2}$  where the electronic clouds are more elongated along the  $z$  direction in comparison with the  $d_{3x^2-r^2}$  and  $d_{3y^2-r^2}$  orbitals. It is noted that, with doping of holes, the saturated orbital

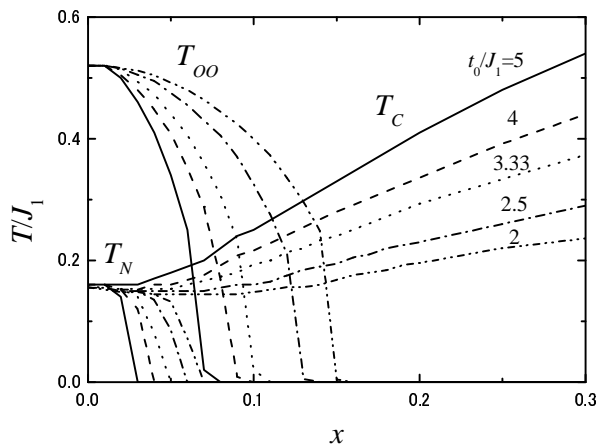


FIG. 8: The spin and orbital phase diagram as functions of  $t_0/J_1$ . The parameter values are chosen to be  $J_2/J_1 = 0.25$  and  $J_{AF}/J_1 = 0.014$ .

moment  $|m_t^{\mu}|$  gradually decreases, and finally disappears at  $x_c$ . On the other hand, the bond variable  $|\chi_t^l|$  grows up from zero at  $x = 0$ . That is, the two FM interactions, i.e. the double exchange interaction based on the kinetic term  $\mathcal{H}_t$  and the superexchange FM one from  $\mathcal{H}_J$ , co-exist. This is consistent with the present experimental results in  $\text{Pr}_{0.75}\text{Ca}_{0.25}\text{MnO}_3$  that the magnitude of the Jahn-Teller distortion, related to the magnitude of the diagonal order parameters  $m_t^{\mu}$ , is significantly reduced in comparison with that in  $\text{PrMnO}_3$ . Unfortunately, in this calculation, this FM phase is not insulating, because the translational symmetry is assumed in the mean field approximation. However, we numerically confirm that the band width of charge carriers, which is proportional to the bond order parameter  $\chi_t^l$ , is much reduced in the orbital ordered FM phase in comparison with that in the FM phase orbital liquid phase. We believe that doped carriers in such a narrow band tend to be localized by other ingredients which are not taken into account in the present model.

We also examine the phase diagram by changing the relative ratio of the kinetic energy and the exchange energy  $t_0/J_{1(2)}$  [Fig. 8]. With decreasing  $t_0/J_{1(2)}$ , the critical hole concentration  $x_c$ , where  $T_{OO}$  disappears, increases and the region of the orbital ordered FM phase is extended to the region with higher  $x$ . On the other hand,  $T_C$  in the FM metallic phase is reduced and  $T_N$  and  $T_C$  become less sensitive to  $x$ . These calculated results may explain a difference of the phase diagrams of  $\text{La}_{1-x}\text{Sr}_x\text{MnO}_3$  (LSMO),  $\text{La}_{1-x}\text{Ca}_x\text{MnO}_3$  (LCMO) and  $\text{Pr}_{1-x}\text{Ca}_x\text{MnO}_3$  (PCMO). The parameter value of  $t_0/J_{1(2)}$  in the calculation is expected to decrease in this order of the materials. The FM-I phase is realized in the regions of  $0.1 < x < 0.15$  for LSMO,  $0.12 < x < 0.22$  for LCMO and  $0.15 < x < 0.3$  for PCMO; the FM-I phase is extended and shifts to the region with higher  $x$ .  $T_C$  in the FM-M phase in LSMO is almost twice of  $T_N$  in  $\text{LaMnO}_3$ . On the other hand, difference between  $T_N$  in

$\text{PrMnO}_3$  and  $T_C$  in PCMO with  $x = 0.3$  is about 30% of the  $T_N$ .

In order to examine the spin dynamics in the orbital ordered FM phase, we calculate the spin stiffness by applying the linear spin wave theory to the model Hamiltonian in Eq. (1). The effective exchange interaction  $J_l^{\text{eff}}$  corresponding to the interaction  $J_l$  along the direction  $l(=x, y, z)$  in the Heisenberg model  $-\sum_{\langle ij \rangle} J_l^{\text{eff}} \vec{S}_i \cdot \vec{S}_j$  is obtained as

$$J_l^{\text{eff}} = \frac{-D_l^t + 2D_l^J}{2S^2}. \quad (19)$$

$D_l^t$  is a stiffness constant arising from the transfer term of the Hamiltonian  $\mathcal{H}_t$  given by

$$D_l^t = xt_0\chi_t^l, \quad (20)$$

and  $D_l^J$  is the one from  $\mathcal{H}_J$  and  $\mathcal{H}_{AF}$  given by

$$D_l^J = -J_l \frac{1}{4} - J_{AF} \frac{9}{4}, \quad (21)$$

with

$$J_x = -\frac{1}{2}(J_1 - 3J_2)(1-x)^2 + \frac{1}{2}(J_1 + J_2) \left( \frac{1}{4}m_t^{z^2} - \frac{3}{4}m_t^{x^2} - 4\chi_t^{x^2} \right) - J_2 m_t^z \quad (22)$$

and

$$J_z = -\frac{1}{2}(J_1 - 3J_2)(1-x)^2 + \frac{1}{2}(J_1 + J_2) \left( \frac{1}{2}m_t^{z^2} - 4\chi_t^{z^2} \right) + 2J_2 m_t^z. \quad (23)$$

Here, we define the average magnitude of the Mn spin as  $S = (1-x)/2 + 3/2$ . The  $x$  dependence of the effective exchange interactions,  $J_x(=J_y)$  and  $J_z$ , are presented in Fig. 9. In the  $A$ -type AF phase near  $x = 0$ ,  $J_z$  is negative and its magnitude is much weaker than that of  $|J_x|$ . This is experimentally confirmed by the inelastic neutron scattering in  $\text{LaMnO}_3$ . With doping of holes, the sign of  $J_z$  is changed into a positive one, and  $J_x$  decreases and  $J_z$  increases. That is, the anisotropy of the exchange interactions is much reduced. This tendency of the  $x$  dependence of the anisotropy of  $J_l^{\text{eff}}$  is consistent with the present neutron scattering experiments in  $\text{Pr}_{1-x}\text{Ca}_x\text{MnO}_3$ , although, in the calculation, the weak anisotropy of  $J^{\text{eff}}$  remains in the orbital ordered FM phase. Such an anisotropy may not be detected due to the coarse resolution of the present neutron scattering experiments.

#### IV. CONCLUSION

We have systematically investigated the nature of the FM-I state of perovskite manganites by a neutron scattering study on a single crystal of  $\text{Pr}_{0.75}\text{Ca}_{0.25}\text{MnO}_3$  and



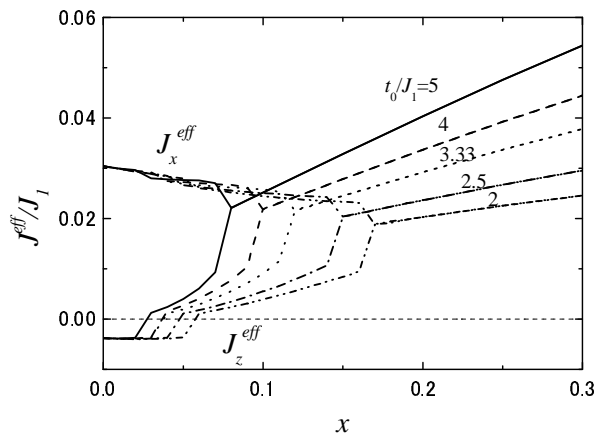


FIG. 9: The  $x$  dependence of the effective exchange interaction  $J_x^{eff}$  and  $J_z^{eff}$ . The parameter values are chosen to be  $J_2/J_1 = 0.25$  and  $J_{AF}/J_1 = 0.014$ .

theoretical calculations. We have found that 1) the insulating behavior is robust against an external magnetic field, 2) the FM moment is almost fully polarized, 3) the Jahn-Teller lattice distortions are strongly suppressed, and 4) the spin exchange interactions are isotropic. These features are against interpretations of insulating behavior based on COs or phase separation, and are consistent to the staggered type orbital ordered state. The spin

stiffness is similar to those observed in other FM-I manganites and has a smaller value than that in the FM-M phase, indicating the ubiquitous origin of the FM-I state. We theoretically construct the comprehensive spin and orbital phase diagram for the FM phase, which can explain the difference of the phase diagrams of several manganites.

Lastly, we should note the importance of our work for the research of the I-M transition or the CMR phenomenon in hole-doped perovskite manganites. Many previous experimental researches focusing attention on the phase separation as an origin of the I-M transition attribute an isotropic phase or a FM phase to a metallic phase. However, the existence of an *isotropic ferromagnetic* insulating phase means one must pay better attention to identifying the metallic phase and consider the effect of the staggered type OO especially in the low-doped region.

### Acknowledgments

This work was supported by a Grant-In-Aid for Scientific Research from the Ministry of Education, Culture, Sports, Science, and Technology, Japan. R. K. was supported by the Japan Society for the Promotion of Science.

\* Present address: Neutron Science Facility, Institute of Materials Structure Science, High Energy Accelerator Research Organization, 1-1 Oho, Tsukuba, Ibaraki 305-0801, Japan; Electronic address: kaji@post.kek.jp.

† Present address: Department of Physics, Columbia University, 538 West 120th Street, New York, NY 10027.

<sup>1</sup> J. Rodríguez-Carvajal, M. Hennion, F. Moussa, A. H. Moudden, L. Pinsard, and A. Revcolevschi, Phys. Rev. B **57**, R3189 (1998).

<sup>2</sup> Y. Murakami, J. P. Hill, D. Gibbs, M. Blume, I. Koyama, M. Tanaka, H. Kawata, T. Arima, Y. Tokura, K. Hirota, and Y. Endoh, Phys. Rev. Lett. **81**, 582 (1998)

<sup>3</sup> M. Imada, A. Fujimori, and Y. Tokura, Rev. Mod. Phys. **70** (1998) 1039.

<sup>4</sup> K. Hirota, N. Kaneko, A. Nishizawa, and Y. Endoh, J. Phys. Soc. Jpn. **65**, 3736 (1996).

<sup>5</sup> F. Moussa, M. Hennion, J. Rodríguez-Carvajal, H. Moudén, L. Pinsard, and A. Revcolevschi, Phys. Rev. B **54**, 15149 (1996).

<sup>6</sup> P. G. de Gennes, Phys. Rev. **118**, 141 (1960).

<sup>7</sup> S. Ishihara, M. Yamanaka, and N. Nagaosa, Phys. Rev. B **56**, 686 (1997).

<sup>8</sup> A. Urushibara, Y. Moritomo, T. Arima, A. Asamitsu, G. Kido, and Y. Tokura, Phys. Rev. B **51**, 14103 (1995).

<sup>9</sup> Michael C. Martin, G. Shirane, Y. Endoh, K. Hirota, Y. Moritomo, and Y. Tokura, Phys. Rev. B **53**, 14285 (1996).

<sup>10</sup> T. G. Perring, G. Aeppli, S. M. Hayden, S. A. Carter, J. P. Remeika, and S.-W. Cheong, Phys. Rev. Lett. **77**, 711 (1996).

<sup>11</sup> Y. Tomioka, A. Asamitsu, H. Kuwahara, Y. Moritomo, and Y. Tokura, Phys. Rev. B **53**, R1689 (1996).

<sup>12</sup> H. Yoshizawa, H. Kawano, Y. Tomioka, and Y. Tokura, Phys. Rev. B **52**, R13145 (1995).

<sup>13</sup> J. Phys. Soc. Jpn. **65**, 1043 (1996).

<sup>14</sup> Pengcheng Dai, J. A. Fernandez-Baca, N. Wakabayashi, E. W. Plummer, Y. Tomioka, and Y. Tokura, Phys. Rev. Lett. **85**, 2553 (2000).

<sup>15</sup> M. Uehara, S. Mori, C. H. Chen, and S.-W. Cheong, Nature (London) **399**, 560 (1999).

<sup>16</sup> D. E. Cox, P. G. Radaelli, M. Marezio, and S.-W. Cheong, Phys. Rev. B **57**, 3305 (1998).

<sup>17</sup> T. Hotta and E. Dagotto, Phys. Rev. B **61**, R11879 (2000).

<sup>18</sup> T. Mizokawa, D. I. Khomskii, and G. A. Sawatzky, Phys. Rev. B **61**, R3776 (2000).

<sup>19</sup> T. Mizokawa, D. I. Khomskii, and G. A. Sawatzky, Phys. Rev. B **63**, 024403 (2000).

<sup>20</sup> Y. Endoh, K. Hirota, S. Ishihara, S. Okamoto, Y. Murakami, A. Nishizawa, T. Fukuda, H. Kimura, H. Nojiri, K. Kaneko, and S. Maekawa, Phys. Rev. Lett. **82**, 4328 (1999).

<sup>21</sup> S. Okamoto, S. Ishihara, and S. Maekawa, Phys. Rev. B **61**, 14647 (2000).

<sup>22</sup> M. v. Zimmermann, C. S. Nelson, J. P. Hill, Doon Gibbs, M. Blume, D. Casa, B. Keimer, Y. Murakami, C.-C. Kao, C. Venkataraman, T. Gog, Y. Tomioka, and Y. Tokura, Phys. Rev. B **64**, 195133 (2001).

<sup>23</sup> L. Vasiliu-Doloc, J. W. Lynn, Y. M. Mukovskii, A. A. Arsenov, and D. A. Shulyatev, J. Appl. Phys. **83**, 7342 (1998).

- <sup>24</sup> Strictly speaking, this position is where the superlattice peak due to the *CE*-type OO is expected. Because it has been confirmed that the OO and CO are intimately related in the *CE*-type CO,<sup>25</sup> we refer the *CE*-type OO peaks as *CE*-type CO peaks in the present paper.
- <sup>25</sup> M. v. Zimmermann, J. P. Hill, Doon Gibbs, M. Blume, D. Casa, B. Keimer, Y. Murakami, Y. Tomioka, and Y. Tokura, Phys. Rev. Lett. **83**, 4872 (1999).
- <sup>26</sup> S. Shimomura, N. Wakabayashi, H. Kuwahara, and Y. Tokura, Phys. Rev. Lett. **83**, 4389 (1999).
- <sup>27</sup> C. P. Adams, J. W. Lynn, Y. M. Mukovskii, A. A. Arsenov, and D. A. Shulyatev, Phys. Rev. Lett. **85**, 3954 (2000).
- <sup>28</sup> Z. Jiráček, S. Krupička, Z. Šimša, M. Dlouhá, and S. Vratislav, J. Magn. Magn. Mat. **53**, 153 (1985).
- <sup>29</sup> Y. Endoh and K. Hirota, J. Phys. Soc. Jpn. **66**, 2264 (1997).
- <sup>30</sup> Pengcheng Dai, J. A. Fernandez-Baca, E. W. Plummer, Y. Tomioka, and Y. Tokura, Phys. Rev. B **64**, 224429 (2001).
- <sup>31</sup> J. A. Fernandez-Baca, Pengcheng Dai, H. Kawano-Furukawa, H. Yoshizawa, E. W. Plummer, S. Katano, Y. Tomioka, and Y. Tokura, Phys. Rev. B **66**, 054434 (2002).
- <sup>32</sup> K. Hirota, N. Kaneko, A. Nishizawa, Y. Endoh, M. C. Martin, and G. Shirane, Physica B **237-238**, 36 (1997).
- <sup>33</sup> S. Ishihara, J. Inoue, and S. Maekawa, Phys. Rev. B **55**, 8280 (1997).
- <sup>34</sup> S. Ishihara and S. Maekawa Phys. Rev. B **58**, 13442 (1998).
- <sup>35</sup> G. Khaliullin and R. Kilian, Phys. Rev. B **61**, 3494 (2000).
- <sup>36</sup> A. M. Oleś and L. F. Feiner, Phys. Rev. B **65**, 052414 (2002).
- <sup>37</sup> K. Hirota, S. Ishihara, H. Fujioka, M. Kubota, H. Yoshizawa, Y. Moritomo, Y. Endoh, and S. Maekawa, Phys. Rev. B **65**, 064414 (2002).